

This is the peer reviewed version of the following article:

Ivañez, I., Sánchez-Saez, S., Garcia - Castillo, S. K., Barbero, E., Amaro, A. M. & Reis, P. N. B. (2020). Impact response of repaired sandwich structures. *Polymer Composites*, 41(8), 3014–3022.

Which has been published in final form at
<https://doi.org/10.1002/pc.25593>

This article may be used for non-commercial purposes in accordance with Wiley Terms and Conditions for Use of Self-Archived Versions.

Impact response of repaired sandwich structures

I. Ivañez^a, S. Sánchez-Saez^a, S.K. Garcia-Castillo^a, E. Barbero^a, A.M. Amaro^b, P.N.B. Reis^c

^a Dep. of Continuum Mechanics and Structural Analysis. University Carlos III of Madrid, Leganés, Spain

^b CEMMPRE, Dep. of Mechanical Engineering, University of Coimbra, Coimbra, Portugal

^c C-MAST, Dep. of Electromechanical Engineering, University of Beira Interior, Covilhã, Portugal

Abstract

The low-velocity impact behaviour of repaired sandwich structures with woven carbon/epoxy face-sheets and Nomex honeycomb core is studied experimentally. First, sandwich plates were subjected to ballistic impacts; the damaged area was removed, filled by nano-enhanced resin and covered by a double-external patch. Afterwards, the repaired sandwich plates were impacted at low-velocity. Peak load and absorbed energy were determined for several impact energies and compared with results for non-repaired (intact) sandwich plates. For all impact energies tested, repaired specimens show higher peak load and lower absorbed energy than the intact ones. Additionally, tested sandwich plates were cut transversally in order to observe the resulting damage, concluding that is different in both configurations, and confirming that it is initiated at higher impact energies in repaired structures.

Keywords: Composites, impact resistance, damage zone.

1. Introduction

Composites continue to replace traditional materials, like steel and aluminium, due to their excellent properties. In this context, due to their superior bending stiffness, better structural capacity in carrying transverse loads, high-energy absorption characteristics and low weight, structural sandwich composites have been widely used in many engineering fields [1, 2].

Composite sandwich structures are composed by two thin laminates (face-sheets) bonded to a thick core of low-density. The face-sheets made of fibre reinforced polymer laminates are used to obtain high in-plane mechanical properties and, in terms of core, the most commonly used materials are metallic, syntactic and polymer foam, honeycomb Nomex and balsa wood [3]. The cores are responsible for separating and fixing the face-sheets, in addition to carrying the transverse shear loads. Of all low -density materials mentioned above, honeycomb structures are very popular in aerospace industry when combined with composite laminate face-sheets to obtain lightweight structural components [4-8]. However, because of their thin face-sheets, sandwich structures are very sensitive to impact events that occur in the service life or in maintenance activities [9, 10].

For low-impact energies, a wide range of damage can be observed, like core buckling and cracking, fibre breakage and debonding between face-sheet and core [11], but the face-sheets can be easily perforated by a projectile when the impact velocity is above certain values [10]. Consequently, due to the loss of strength and reliability of composite components, internal damage can lead to a catastrophic failure [12] or even as a result of the passage of water and/or moisture into the structures, the mechanical performance may deteriorate [13].

For example, Akatay et al. [14] analysed the effect of multi-impacts in sandwich structures with glass fibre/epoxy face-sheets and honeycomb core. They showed that the number of impacts that cause the complete perforation of the samples augments with the decrease in impact energy. Rupp et al. [15] studied the sandwich structures behaviour, and they found that face-sheets with higher fibre area weight promote larger maximum force values, but the deformation is largely influenced by the core. Sun et al. [16] analysed the behaviour and failure mechanisms of sandwich plates with honeycomb core subjected to high-velocity impact by an experimental and numerical study. These authors have observed that the ballistic limit of sandwich panels increases almost linearly with increasing face-sheet thickness, smaller cell sizes are responsible for greater perforation resistance whereas the core height shows to have a very small effect on this parameter. Simultaneously, with the augment of face-

sheet thickness, the maximum deformation in thickness direction diminishes while the deformation area, which is related to bending deflection, increases on both face-sheets of sandwich structures. According to Xiamonin et al. [17] a well-designed sandwich plate should have appropriate core geometry and arrangement to support the impact load intensity. However, if literature reports several works on the mechanical response of sandwich structures with honeycomb core under impact loading, few studies can be found for perforation failure.

The damage generated in sandwich structures due to ballistic impacts is not widespread and extensive [10], and therefore a structural repair is a feasible solution, rather than replacement of the component, because in many cases the costs are significantly lower [18, 19]. In this context, the stiffness and strength of the damaged component must be restored to give its original service condition back as possible. For this purpose, different techniques are available and the most common are mechanical bolts, injection repair and adhesively bonded-patch [20]. The first technique has limited use, because it induces stress concentrations in the laminate, while the second one does not restore completely the laminate tensile strength. Therefore, adhesive patch repair overcomes these limitations [4] and, basically, literature reports essentially two types of patch configurations: scarf patches and overlap patch [7, 21]. Both guarantee a safe and adequate repair, but regardless of the first methodology to promote benefits in terms of aerodynamic outline modifications and little bending moments, it is complex to make, demands special devices and is time-consuming. In terms of external patch, this technique is easier to apply than a scarf repair, but it produces a stress concentration at the patch borders, because of the change in the aerodynamic outline and, if the patch is very thick, the bending moments and stiffness induced may be a disadvantage to be accepted [22-26].

Independently of the fact that repairs on composite structures (monolithic and sandwich) with adhesives and composite patches are being extensively accepted and reported in the open literature, inclusively after the ballistic impact [27], authors did not find studies on impact behaviour of sandwich composites that were repaired after ballistic impact. Therefore, the main goal of this work

is to study the low-velocity impact response of repaired honeycomb sandwich structures by the external patch method. Due to its simplicity, the external overlap is widely used on internal component repairs such as formers, bulkheads and inner skins [28]. However, while scarf repair is preferred due to aerodynamic cleanliness and minimising of moment induced failure modes, the external patch provides very satisfactory results for damages that are repaired according to the Aircraft Maintenance and Repair Manual [19, 28, 29]. The composite sandwich plates were based on face-sheets of woven carbon fibre/epoxy and core of Nomex honeycomb. After ballistic impact, the damage zone is filled with a nano-enhanced epoxy resin and, finally, two external patches (with the same thickness of the face-sheets) are bonded to the repaired sample. The low-velocity impact resistance was evaluated in terms of load- and energy-time plots, as well as through the determination of the peak load and absorbed energy during the impact tests. In order to analyse the damage, several specimens were cut transversely after impact. All results were compared with those of a previous study on un-repaired sandwich plates subjected to low-velocity impact, and significant differences were obtained.

2. Materials and Experimental Procedure

As consequence of the wide use in the aerospace industry, composite sandwich plates based on face-sheets of plain weave carbon fibre/epoxy (AS4/8552) at 0°, 1.2 mm thick, and a core of Nomex honeycomb (HRH-10-1/8-3.0), with a thickness of 10 mm, were studied in the present work. Specimens were supplied by a research centre in accordance with the standards of the aerospace industry. More details about this material and respective properties can be found in [30].

Previously, specimens with 120×120 mm² were subjected to ballistic impacts that produced the complete perforation (at impact velocities in the range of 200 - 500 m/s), where metallic spheres with 7.5 mm of diameter and 1.7 g of weight were used. Fig. 1 shows typical damages after impact and after removal of the face-sheets. In terms of face-sheets, it is notorious the damage confined to a hole

produced on the front face-sheet (Fig. 1a) by the projectile, and a hole with some delaminated layers on the back face-sheet (Fig.1b). On the other hand, in terms of core, the Nomex was perforated with dimensions very close to the projectile (Fig. 1c).

After analysing the damage caused by ballistic impact and concluding that internally it is practically confined to a hole, its repair consisted of filling it with resin enhanced by carbon nanofibers (Fig. 1d). In fact, the materials used on the repairs should be suggested by the Aircraft Maintenance and Repair Manual [30], but nowadays it is common to use aeronautical resins with different fillers [19, 31], specially nano-enhanced resins [26]. Literature reports significant benefits when resins with different fillers are introduced into the depression due to the higher rigidity of the specimens repaired [26, 31], besides other advantages such as better thermal and electrical properties when carbon nanofibers are added [32]. Finally, two external patches with the same thickness were bonded with an Araldite[®] 420 A/B adhesive (Fig. 1e). The laminates used as patches are composed by six layers of Texipreg[®] HS 160 REM, supplied by SEAL, with the sequence of [0/90]₃.

A SR 8100 epoxy resin and a SD 8824 hardener, both supplied by Sicomin, were used to fill the depression/hole. Resin and carbon nanofibers (CNFs) were mixed with resource to an electric mixer at 1000 rpm and, simultaneously, subjected to ultrasonic bath sonicator. The CNFs content was 0.75 wt. % of the resin-hardener mixture, since it is the best quantity for this epoxy system according with previous studies. The nano-enhanced resin was subjected to degassing and later the hardener agent was added. To avoid air bubbles, special care was taken in this mixing process. After filled the depression, the samples were subjected to cure at room temperature during 24 h, and later post-cure in an oven at 40 °C for 24 hours, according to manufacturer. The last step involved the bonding of the external patches (40×40×1 mm³) to the parent laminates (120×120×12.4 mm³) and, to get the best adhesion, all components were previously cleaned/degreased with methyl-ethyl-ketone.

Low-velocity impact tests were carried out using a drop weight tower, CEAST Fractovis. For this study, a special support device was manufactured to test sandwich specimens of 120 x 120 mm², which assures that the specimen edges are clamped (Fig. 2).

An impactor with a hemispherical nose of 20 mm in diameter and mass of 3.62 kg was used. The tower has an anti-rebound system to avoid successive impacts in the same specimen. The impact velocity was determined by a photocell placed close to the impact point. A piezoelectric load cell is located in the impactor to calculate the contact load between impactor and specimen. From this cell, a record of the variation of contact force was obtained for each test. Using basic equations of the dynamic equilibrium of the impactor it is possible to estimate the acceleration, velocity, displacement and energy of the impactor by a well-known integration process [33, 34].

The impact energies used were 10, 15, 20, 25 and 30 J, which were previously selected to avoid perforation of the specimens. This range of impact energies correspond to velocities from 2.27 m/s to 3.97 m/s. For each condition, at least, three specimens were tested at room temperature. Finally, to identify the damage produced by impact on baseline and repaired specimens, they were cut in the point of impact by a diamond disc. The surfaces were polished with sandpaper of fine grain. The cutting process was made by water as refrigerant to avoid generate additional damage in the specimens.

3. Results and Discussion

Fig. 3 shows representative force-time curves for all impact energies tested in this study. Two types of curves have been observed: sinusoidal curves and curves with a sudden drop in the load. For impact energies below 20 J all force-time curves show a sinusoidal shape. This behaviour is typically related to low damage extension, in which the main failure mechanism is controlled by matrix damage [14]. The drop in the load that appears at impact energies over 20 J (Fig. 3b) is about 55% of the peak load and remains approximately constant when the impact energy increases. This drop in load is also has

been reported by other authors when studying in monolithic laminates, and increases with the laminate thickness. For example, in laminates 2 mm thick is around 16% [9], whereas in laminates of 9 mm is around 40% [35]. In monolithic laminates, Quaresimin et al. [36] suggest that the load for which this sudden drop appear is independent of the impact energy.

From the load-time record, the variation of the impactor energy was estimated. The energy-time curves present the typical shape of a low-velocity impact test that grow to a maximum value (equal to the impact energy) and decrease until a constant value, which corresponds to the energy absorbed by the specimen [37-39]. The absorbed energy increases with the impact energy, as displayed in Fig. 4. As observed in load-time curves, the absorbed energy presents two trends: below impact energy of 20 J the energy absorbed by the specimens is around 50%, and over 20 J this value is higher than 60%.

A detailed analysis carried out in specimens impacted at 20 J reported a transition between the two types of curves, some specimens showed a sinusoidal load variation (curve “a” at 20J) and other presented a drop in load and an increment in contact time (curve “b” at 20J). The drop in load implies a damage progression the specimen and the activation of other failure mechanisms, such as fibre-breakage and delamination growth, that produce an instant decrement of the stiffness of the specimen [35, 40, 41]. In addition, in repaired specimens impacted at 20 J, a significant increase in the absorbed energy is observed depending on the type of load-time curve obtained in the test (Figure 4): for sinusoidal curves the energy absorption is 43.5%, whereas for the other type of curves this value is around 60%. The increase of the contact time in the latter curves (around 15%) is linked to an increment of damage in the specimen that reduces the stiffness and augments the impactor displacement. The change in behaviour suggests that for the sandwich structures analysed, the threshold energy from which new damage mechanisms are activated is about 20 J.

From load-time and energy-time curves, the peak load and absorbed energy as a function of the impact energy were determined. In Fig. 5 to 7 these variables are compared with results of baseline

specimens (intact un-repaired sandwich plates). The baseline specimens data correspond to a previous work that includes both experimental and numerical results. Detailed information on the experimental tests and the numerical model can be found in [30].

Peak load shows the same trend in baseline and repaired sandwich structures (Fig. 5) and increases almost linearly until reaching a maximum value, which corresponds to the critical impact energy. From this impact energy, it remains practically constant. This behaviour is consistent with the open literature, where the peak load augments with increasing impact energy [37, 42, 43]. According to Hosur et al. [44] the peak load rises almost linearly with higher impact energies, where the differences observed in terms of maximum loads are consequence of the different failure modes activated [45]. In the case of repaired sandwich plates, the critical impact energy coincides with the threshold energy (20 J), which is the impact energy from which the load-time curves changed their sinusoidal shape caused by the activation of other damage mechanisms in the upper face-sheet. In baseline specimens this critical energy is lower, around 10 J. The peak load values are very different: baseline specimens present a value of around 2 kN, and the repaired specimens 7.4 kN. This increment is related to the greater stiffness of the repaired specimens, and differences are more visible for the higher impact energies used in this work.

Generally, the energy absorption is lower in repaired specimens (Fig. 6). The absorbed energy of baseline specimens and repaired specimens for an impact energy of 10 J is 84% and 40%, respectively (Fig. 7). At 30 J repaired specimens present an energy absorption of 68%, whereas under the same conditions baseline specimens have practically absorbed all impact energy (97%). This behaviour is due to the lower level of damage and greater stiffness of repaired specimens, as differences between the energy absorption of baseline and repaired specimens decrease with increasing damage. In baseline specimens, the honeycomb core is also extensively damaged, thus different damage mechanisms that lead to higher energy absorption are activated.

In addition, as depicted in Fig. 6 and 7, the absorbed energy of repaired specimens presents two different trends, above and below an impact energy around 20 J, and between both zones there is a sudden increment that is not observed in results of baseline specimens. This change in behaviour is related to the debonding of the patch in the repaired specimens, which was observed via cross-sectional view (Fig. 10).

The damage evaluation in the specimens was carried out by visual inspection. For the sake of brevity, two representative samples of the repaired specimens were selected: one impacted at 10 J, and the other at 30 J. Afterwards, a baseline specimen impacted at 10 J was analysed. The specimens were transversely cut through the point of impact, and images were obtained with a stereo-optic microscope (KYOWA OPTICAL SDZ-TR-P) equipped with a Basler acA2440-35uc camera (Fig. 8).

In the cross-sectional view of the repaired specimen impacted at 10 J no damage was observed in the core, face-sheets or filler material. By contrast, the baseline specimen impacted at the same impact energy level shows extensive damage in both the upper face-sheet and core (Fig. 9); under the point of impact, the failure of the upper face-sheet is complete, and some damage was detected in the lower face-sheet. Note that the honeycomb core is extensively crushed.

For an impact energy of 30 J, the damage was developed as patch debonding on the lower face-sheet (Fig. 10); however, no clear damage is observed in the upper face-sheet (only a small indentation). In addition, some cracks appear in the filling material around the area close to the impact point.

4. Conclusions

In the present work, the low-velocity impact behaviour of repaired sandwich structures, previously damaged by ballistic impacts, was investigated through experimental tests carried out in a drop-weight tower. From each test, the peak load and absorbed energy were estimated. These parameters were compared with those obtained from a previous study of the authors on un-repaired sandwich

structures subjected to low-velocity impact under the same conditions. Results obtained from these sandwiches structures, called baseline specimens, were used as reference.

The peak load in repaired sandwich structures is higher than in baseline specimens. By contrast, the latter specimens absorb more energy than the repaired ones. This behaviour was observed in a broad range of impact energies, from 5 to 30 J, and it is related to the lower level of damage that appears in repaired specimens. For example, for an impact energy of 10 J the absorbed energy is around 84% for baseline specimens, and only 40% in the case of repaired sandwich structures. For an impact of 30 J, this difference is more significant as values for absorbed energy are 97% and 68% for baseline and repaired specimens, respectively.

Extensive damage was detected in both face-sheet and core in baseline specimens, even when they are subjected to an impact of 10 J. On the other hand, no damage was identified for repaired sandwiches when subjected to the same impact energy level, neither in the core and nor the face-sheets. At an impact energy of 30 J, some cracks appear around the area of impact in repaired specimens. However, no significant damage is distinguished in the upper face-sheet, and only patch debonding is noticed on the lower face-sheet.

Therefore, it can be concluded that repaired sandwich structures offer greater impact resistance, which can result in great benefits in structural and economic terms. This is in good agreement with the open literature, due to the higher rigidity of the specimens repaired obtained with nano-enhanced resins.

Acknowledgement

The authors wish to acknowledge the financial support of the Ministerio de Economía, Industria y Competitividad of Spain (project DPI2017-86324-R) and the Fundação para a Ciência e Tecnologia of Portugal (project UID/EMS/00285/2013).

References

- [1] Grogan J, Tekalur SA, Shukla A, Bogdanovich A, Coffelt RA. Ballistic resistance of 2D and 3D woven sandwich composites. *J Sandw Struct Mater* 2007; 9: 283–302.
- [2] Kiratisaevee, H. and Cantwell, W. J. The impact response of aluminum foam sandwich structures based on a glass fiber-reinforced polypropylene fiber-metal laminate. *Polym Compos* 2004, 25: 499-509.
- [3] Reis PNB, Santos P, Ferreira JAM, Richardson MOW. Impact response of sandwich composites with nano-enhanced epoxy resin. *J Reinf Plast Comp* 2013; 32: 898–906.
- [4] Katnam KB, da Silva LFM, Young TM. Bonded repair of composite aircraft structures: A review of scientific challenges and opportunities. *Prog Aerosp Sci* 2013; 61: 26–42.
- [5] Ivañez I, Barbero E, Sanchez-Saez S. Analytical study of the low-velocity impact response of composite sandwich beams. *Compos Struct* 2014; 111: 459–67.
- [6] Yamashita M, Gotoh M. Impact behavior of honeycomb structures with various cell specifications - Numerical simulation and experiment. *Int J Impact Eng* 2005; 32: 618–30.
- [7] Griškevičius P, Zeleniakienė D, Leišis V, Ostrowski M. Experimental and numerical study of impact energy absorption of safety important honeycomb core sandwich structures. *Materials Science* 2010; 16: 119–23.
- [8] Sun G, Chen D, Huo X, Zheng G, Li Q. Experimental and numerical studies on indentation and perforation characteristics of honeycomb sandwich panels. *Compos Struct* 2018; 184: 110–24.
- [9] Ivañez I, Garcia-Castillo SK, Sanchez-Saez S, Barbero E. Experimental study of the impact behaviour of repaired thin laminates with double composite patch. *Mech Adv Mater Struct* 2018; doi: 10.1080/15376494.2018.1524952 (in press).
- [10] García-Castillo, S. K., Buitrago, B. L. and Barbero, E. Behavior of sandwich structures and spaced plates subjected to high-velocity impacts. *Polym Compos* 2011, 32: 290-296.
- [11] Abrate S. Localized impact on sandwich structures with laminated facings. *Appl Mech Rev* 1997; 50: 69–82.
- [12] Ude AU, Ariffin AK, Azhari CH. Impact damage characteristics in reinforced woven natural silk/epoxy composite face-sheet and sandwich foam, coremat and honeycomb materials. *Int J Impact Eng* 2013; 58: 31–8.
- [13] Liu L, Feng H, Tang H, Guan Z. Impact resistance of Nomex honeycomb sandwich structures with thin fibre reinforced polymer facesheets. *J Sandw Struct Mater* 2018; 20: 531–52.

- [14] Akatay A, Bora MO, Çoban O, Fidan S, Tuna V. The influence of low velocity repeated impacts on residual compressive properties of honeycomb sandwich structures. *Compos Struct* 2015; 125: 425–33.
- [15] Rupp P, Imhoff J, Weidenmann KA. Low-velocity impact properties of sandwich structures with aluminum foam cores and CFRP face sheets. *J Compos Sci* 2018; 2: 24.
- [16] Sun G, Chen D, Wang H, Hazell PJ, Li Q. High-velocity impact behaviour of aluminium honeycomb sandwich panels with different structural configurations. *Int J Impact Eng* 2018; 122: 119–36.
- [17] Xiaomin M, Xin L, Shiqiang L, Rujiang L, Zhihua W, Guiying W. Blast response of gradient honeycomb sandwich panels with basalt fiber metal laminates as face-sheets. *Int J Impact Eng* 2019; 123: 126–39.
- [18] Anoshkin AN, Zuiko VY, Tashkinov MA, Silberschmidt VV. Repair of damage in aircraft composite sound-absorbing panels. *Compos Struct* 2015; 120: 153–66.
- [19] Balcı O, Çoban O, Bora MÖ, Akagündüz E, Yalçın EB. Experimental investigation of single and repeated impacts for repaired honeycomb sandwich structures. *Mat Sci Eng A-Struct* 2017; 682: 23–30.
- [20] Bathia GS, Andrew JJ, Arockiarajan A. Experimental investigation on compressive behaviour of different patch–parent layup configurations for repaired carbon/epoxy composites. *J Compos Mater* 2019; doi.org/10.1177/0021998318822706 (in press).
- [21] Falzon, BG. GARTEUR AG-28: Impact damage and repair of composite structures. Imperial College London, London; 2006.
- [22] Oztelcan C, Ochoab OO, Martin J, Sem K. Design and analysis of test coupons for composite blade repairs. *Compos Struct* 1997; 37: 185–93.
- [23] Whittingham B, Baker AA, Harman A, Bitton D. Micrographic studies on adhesively bonded scarf repairs to thick composite aircraft structure. *Compos Part A-Appl S* 2009; 40: 1419–32.
- [24] Ivañez I, Garcia-Castillo SK, Sanchez-Saez S, Barbero E. Analysis of the impact location on damage tolerance of bonded-repaired composite laminates. *Polym test* 2019; doi: <https://doi.org/10.1016/j.polymertesting.2019.106000>.
- [25] Soutis C, Duan D-M, Goutas P. Compressive behaviour of CFRP laminates repaired with adhesively bonded external patches. *Compos Struct* 1999; 45: 289–301.
- [26] Coelho SRM, Reis PNB, Ferreira JAM, Pereira AM. Effects of external patch configuration on repaired composite laminates subjected to multi-impacts. *Compos Struct* 2017; 168: 259–65.
- [27] Hosur MV, Vaidya UK, Myers D, Jeelani S. Studies on the repair of ballistic impact damaged S2-glass/vinyl ester laminates. *Compos Struct* 2003; 61: 281–90.

- [28] Irving, PE, Soutis C. *Polymer Composites in the Aerospace Industry*. Woodhead Publishing Series in Composites Science and Engineering: Number 50, Elsevier, Cambridge, United Kingdom, 2015.
- [29] Performance Specification- Technical Manuals: Aircraft Battle Damage Assessment and Repair, MIL-PRF-87158B, November 1996.
- [30] Ivañez I, Moure MM, Garcia-Castillo SK, Sanchez-Saez S. The oblique impact response of composite sandwich plates. *Compos Struct* 2015; 133: 1127–36.
- [31] Andrew JJ, Arumugam V, Saravanakumar K, Dhakal HN, Santuli C. Compression after impact strength of repaired GFRP composite laminates under repeated impact loading. *Compos Struct* 2015; 133: 911–20.
- [32] Chatterjee A, Alam K, Klein P. Electrically conductive carbon nanofiber composites with high-density polyethylene and glass fibers. *Mater Manuf Process* 2007; 22: 62-5.
- [33] Belingardi G, Vadori R. Low velocity impact tests of laminate glass-fiber-epoxy matrix composite material plates. *Int J Impact Eng* 2002; 27: 213–29.
- [34] Sánchez-Sáez S, Barbero E, Navarro C. Analysis of the dynamic flexural behaviour of composite beams at low temperature. *Compos Sci Technol* 2007; 67: 2616–32.
- [35] Schoeppner G.A. and Abrate S., Delamination threshold loads for low velocity impact on composite laminates, *Compos. Part A: Appl. S* 2000; 31: 903–15.
- [36] Quaresimin M, Ricotta M, Martello L, Mian S. Energy absorption in composite laminates under impact loading. *Composites: Part B* 2013; 44: 133–40.
- [37] Reis PNB, Ferreira JAM, Zhang ZY, Benameur T, Richardson MOW. Impact response of kevlar composites with nanoclay enhanced epoxy matrix. *Compos Part B* 2013; 46: 7–14.
- [38] Reis PNB, Ferreira JAM, Zhang ZY, Benameur T, Richardson MOW. Impact strength of composites with nano-enhanced resin after fire exposition. *Compos Part B* 2014; 56: 290–5.
- [39] Scarponi C, Schiavoni E, Sánchez-Sáez S, Barbero E, Sarasini F. Polypropylene/hemp fabric reinforced composites: Manufacturing and mechanical behaviour. *J Biobased Mater Bio* 2012; 6(4):361-369.
- [40] Zhou J, Liao B, Shi Y, Zuo Y, Tuo H, Jia L. Low-velocity impact behavior and residual tensile strength of CFRP Laminates. *Composites Part B* 2019; 161: 300–13.
- [41] Rilo N.F. and Ferreira L.M.S., Experimental study of low-velocity impacts on glass-epoxy laminated composite plates, *Int. J. Mech. Mater. Des* 2008; 4: 291–300.
- [42] Iqbal K, Khan S-U, Munir A, et al. Impact damage resistance of CFRP with nanoclay-filled epoxy matrix. *Compos Sci Technol* 2009; 69: 1949–57.

- [43] Reis PNB, Ferreira JAM, Santos P, et al. Impact response of Kevlar composites with filled epoxy matrix. *Compos Struct* 2012; 94: 3520–28.
- [44] Hosur MV, Chowdhury F and Jeelani S. Low-velocity impact response and ultrasonic NDE of woven carbon/epoxy–nanoclay nanocomposites. *J Compos Mater* 2007; 41: 2195–212.
- [45] Gustin J, Joneson A, Mahinfalah M, et al. Low velocity impact of combination Kevlar/carbon fiber sandwich composites. *Compos Struct* 2005; 69: 396–406.

FIGURE CAPTION

Fig. 1. Composite sandwiches repaired: a) Front face-sheet aspect after ballistic impact; b) Back face-sheet aspect after ballistic impact; c) Core damaged aspect; d) Damage filled by nano-enhanced resin; e) External patch aspect covering the damage.

Fig. 2. Special device to support the specimen.

Fig. 3. Load vs. time curves at several impact energies.

Fig. 4. Energy vs. time curves at several impact energies.

Fig. 5. Peak load vs. impact energy.

Fig. 6. Absorbed energy vs. impact energy

Fig. 7. Percentage of absorbed energy vs. impact energy

Fig. 8. Representative damage in baseline and repaired specimens.

Fig. 9. Damage in a baseline sandwich specimen impacted at 10 J, a) Global view, b) Zone I: complete failure, b) Zone II: undamaged, c) Zone III: undamaged, and d) Zone IV: interlaminar damage.

Fig. 10. Damage in a repaired sandwich specimen impacted at 30 J, a) Global view, b) Zone I: impact indentation, b) Zone II: patch debonding, c) Zone III: cracks.

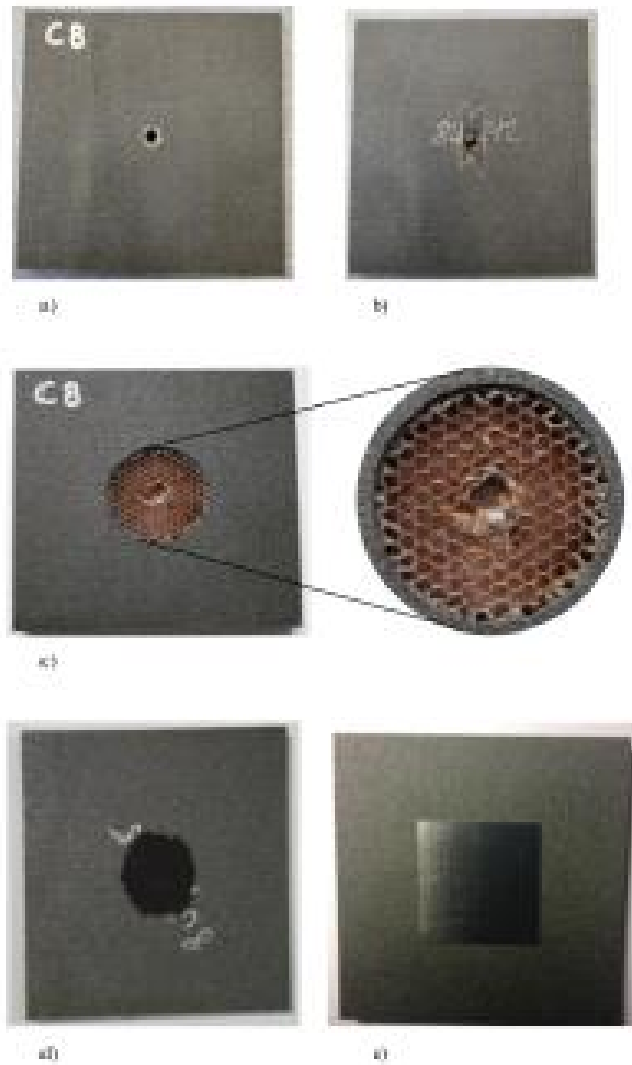


Fig.1. Composite sandwiches repaired: a) Front face-sheet aspect after ballistic impact; b) Back face-sheet aspect after ballistic impact; c) Core damaged aspect; d) Damage filled by nano-enhanced resin; e) External patch aspect covering the damage.

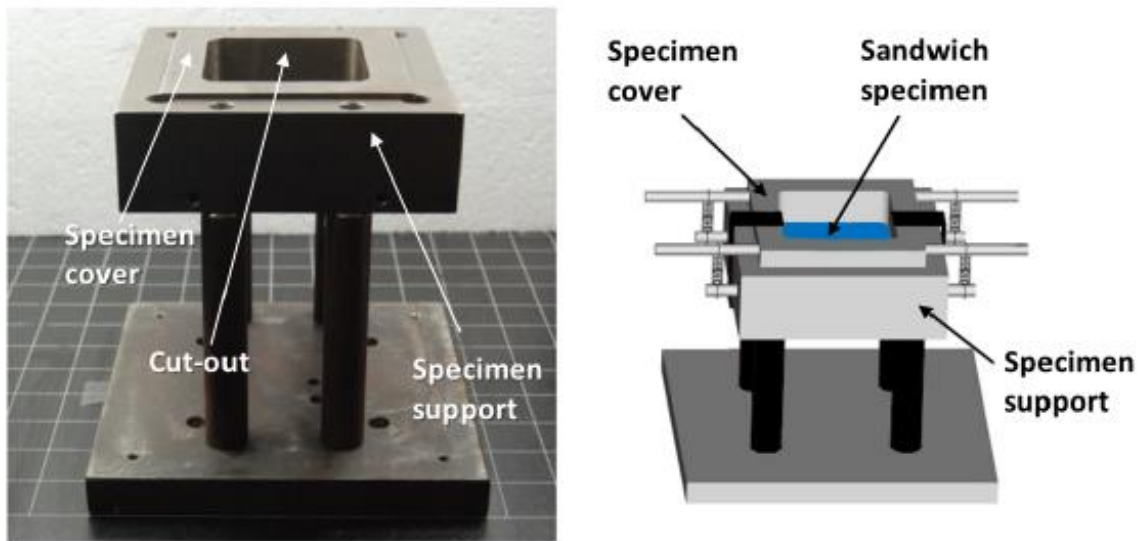


Fig.2. Special device to support the specimen.

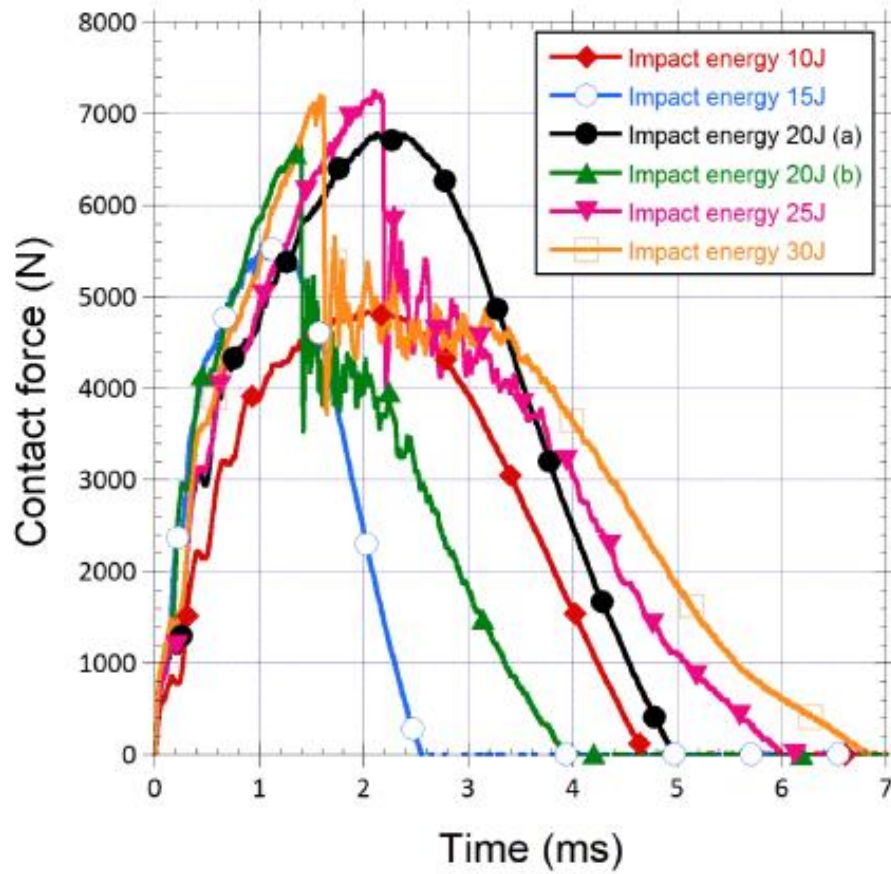


Fig. 3. Load vs. time curves at several impact energies.

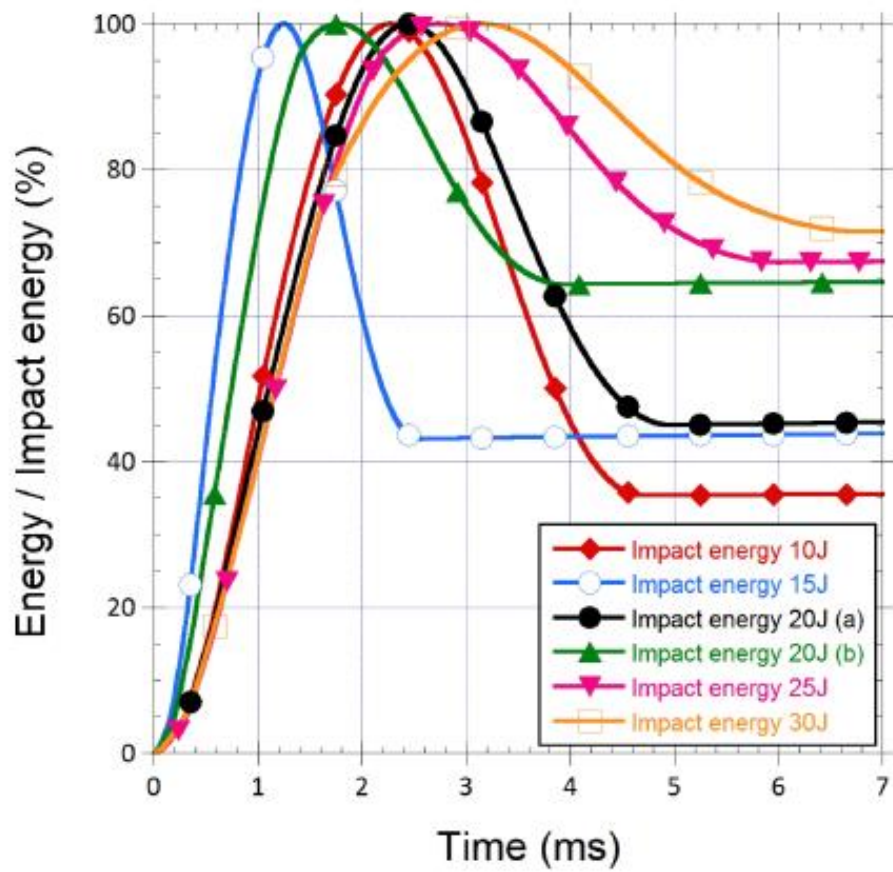


Fig. 4. Energy vs. time curves at several impact energies.

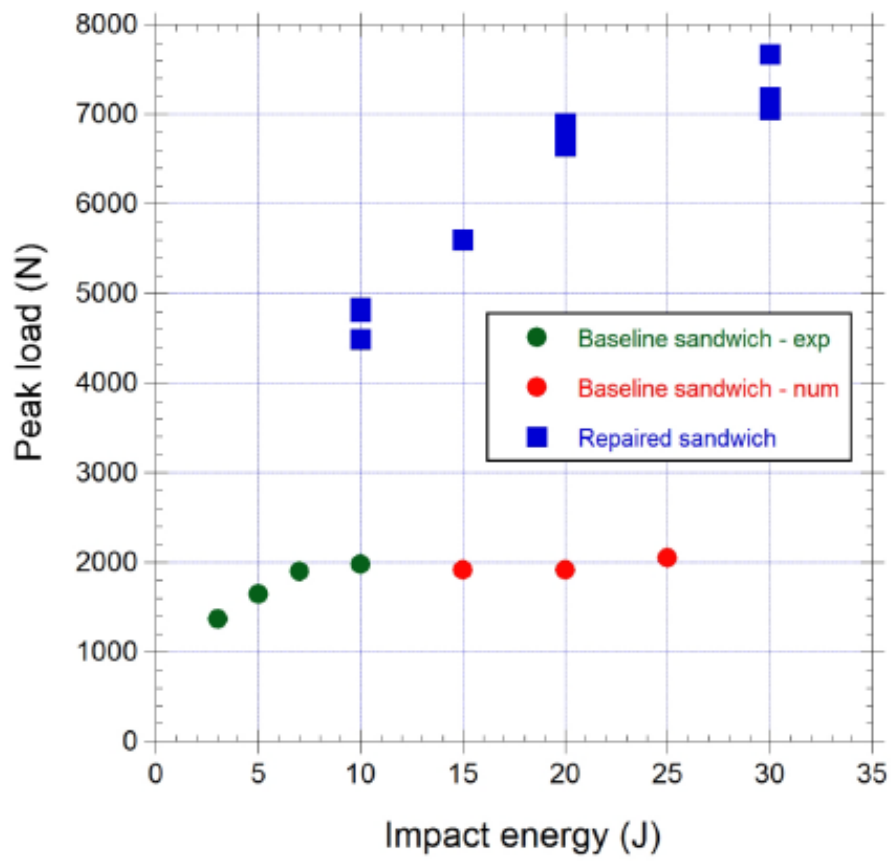


Fig. 5. Peak load vs. impact energy.

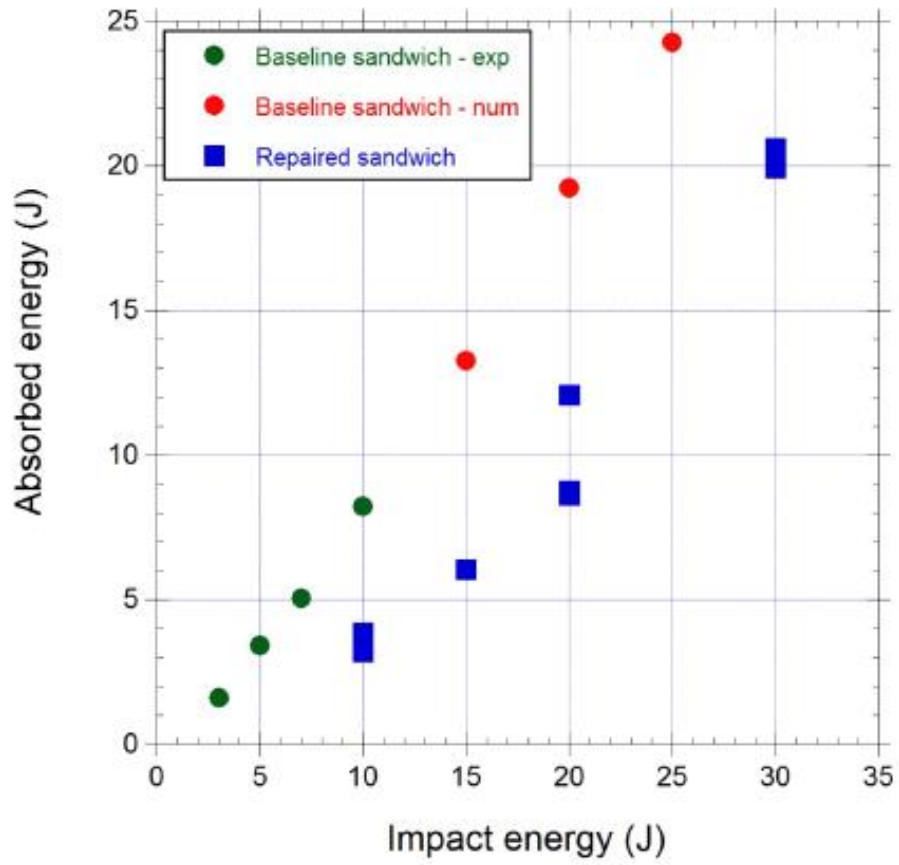


Fig. 6. Absorbed energy vs. impact energy.

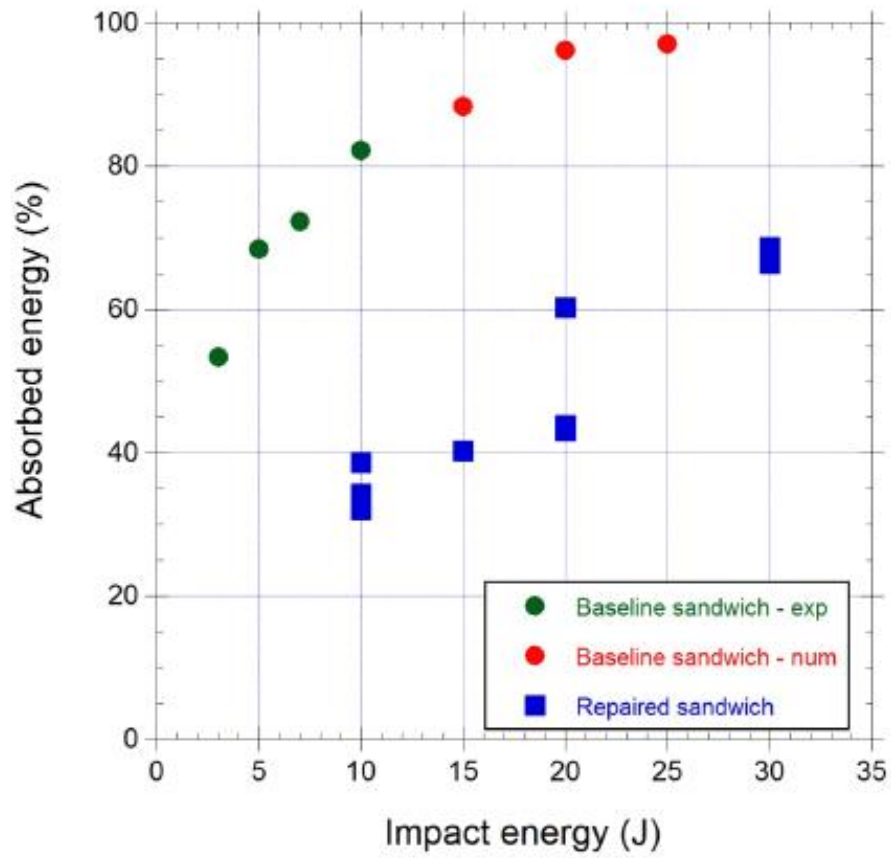


Fig. 7. Percentage of absorbed energy vs. impact energy.



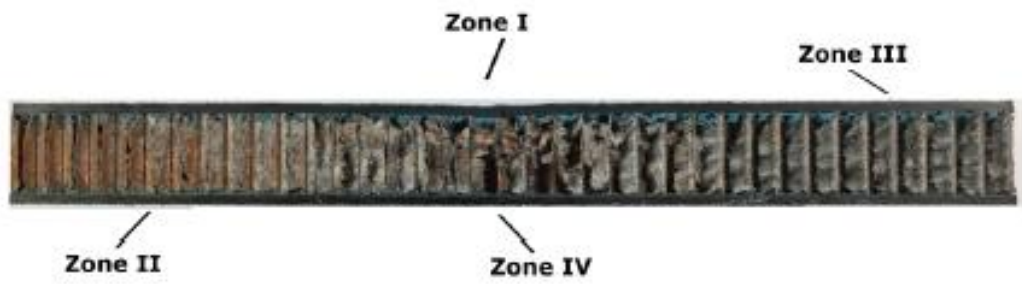
Fig. 8. Representative damage in baseline and repaired specimens, a) Baseline: Impact energy 10 J, b) Repair: Impact energy 10 J, c) Repair: Impact energy 30 J.



Fig. 8. Representative damage in baseline and repaired specimens, a) Baseline: Impact energy 10 J, b) Repair: Impact energy 10 J, c) Repair: Impact energy 30 J.



Fig. 8. Representative damage in baseline and repaired specimens, a) Baseline: Impact energy 10 J, b) Repair: Impact energy 10 J, c) Repair: Impact energy 30 J.



Caption : Fig. 9. Damage in a baseline sandwich specimen impacted at 10 J, a) Global view, b) Zone I: complete failure, c) Zone II: undamaged, d) Zone III: undamaged, and e) Zone IV: interlaminar damage.

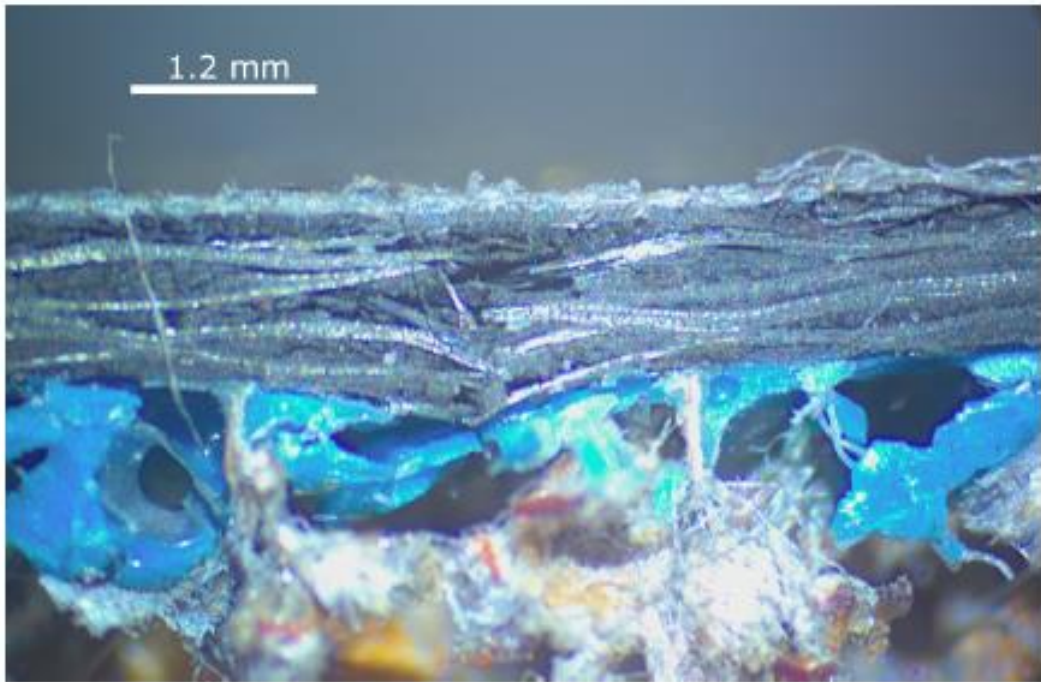


Fig. 9. Damage in a baseline sandwich specimen impacted at 10 J, a) Global view, b) Zone I: complete failure, c) Zone II: undamaged, d) Zone III: undamaged, and e) Zone IV: interlaminar damage.

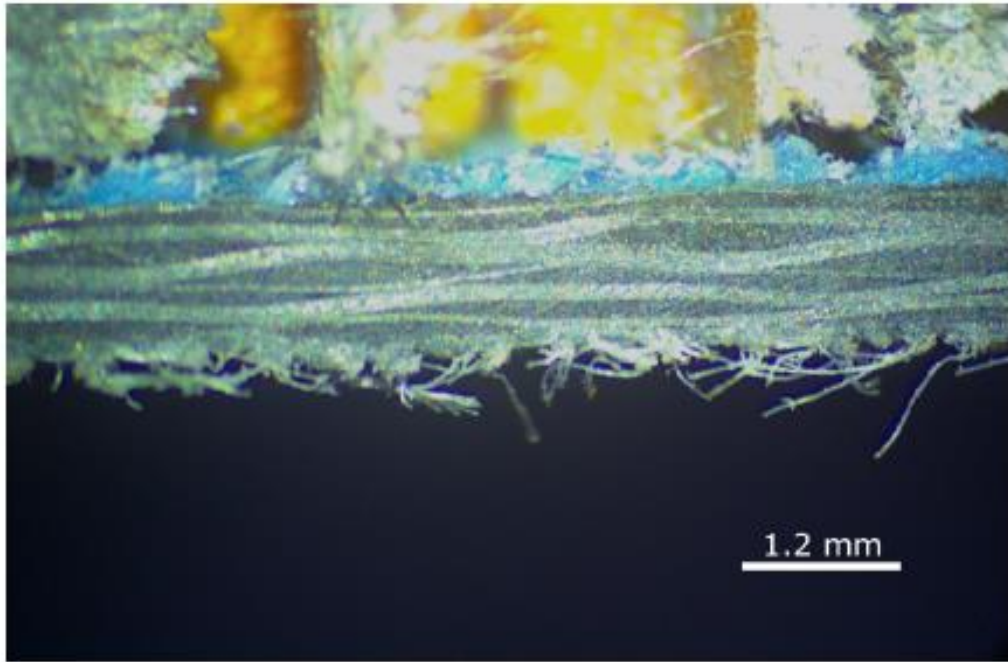


Fig. 9. Damage in a baseline sandwich specimen impacted at 10 J, a) Global view, b) Zone I: complete failure, c) Zone II: undamaged, d) Zone III: undamaged, and e) Zone IV: interlaminar damage.

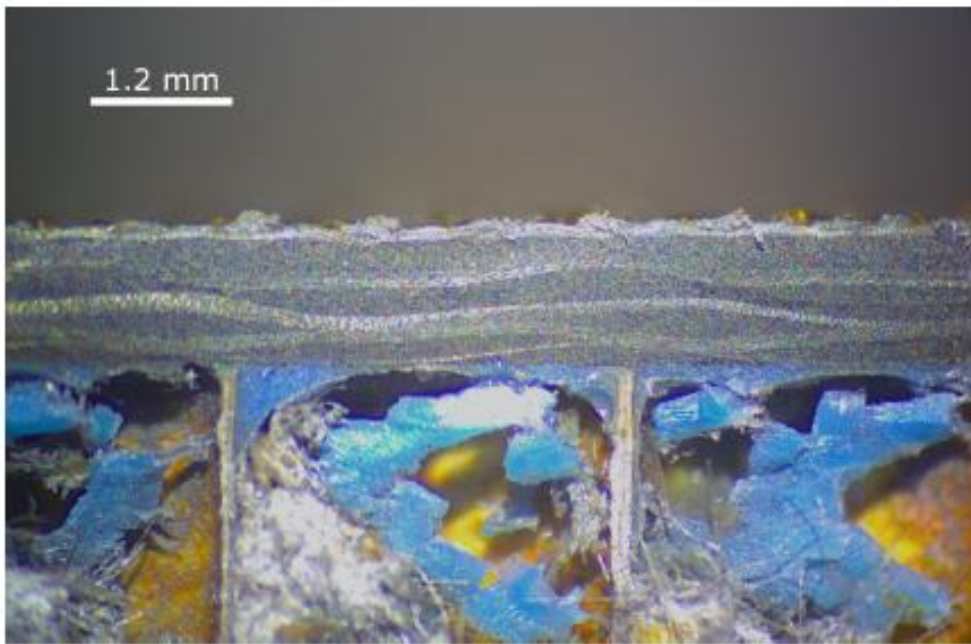


Fig. 9. Damage in a baseline sandwich specimen impacted at 10 J, a) Global view, b) Zone I: complete failure, c) Zone II: undamaged, d) Zone III: undamaged, and e) Zone IV: interlaminar damage.

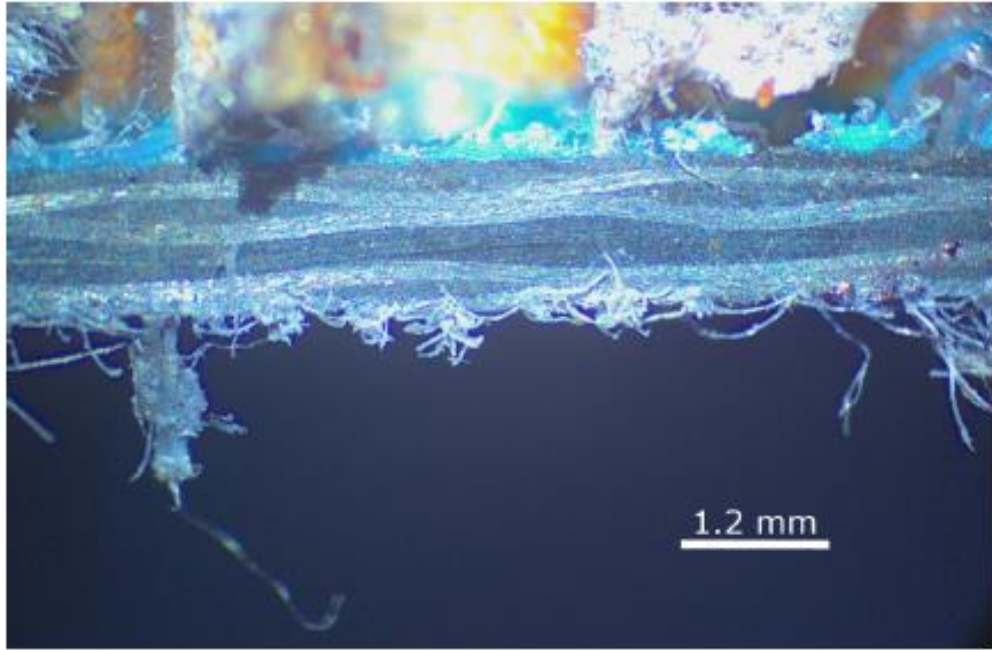


Fig. 9. Damage in a baseline sandwich specimen impacted at 10 J, a) Global view, b) Zone I: complete failure, c) Zone II: undamaged, d) Zone III: undamaged, and e) Zone IV: interlaminar damage.

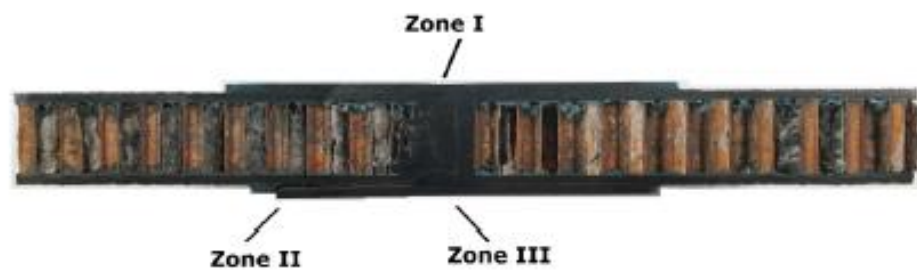


Fig. 10. Damage in a repaired sandwich specimen impacted at 30 J, a) Global view, b) Zone I: impact indentation, c) Zone II: patch debonding, d) Zone III: cracks.

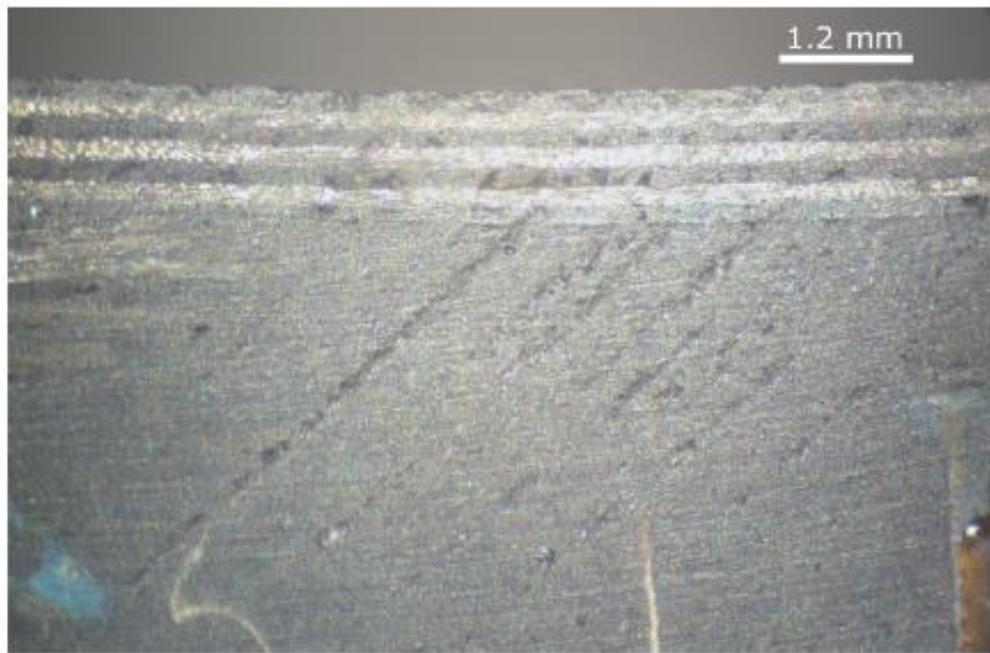


Fig. 10. Damage in a repaired sandwich specimen impacted at 30 J, a) Global view, b) Zone I: impact indentation, c) Zone II: patch debonding, d) Zone III: cracks.

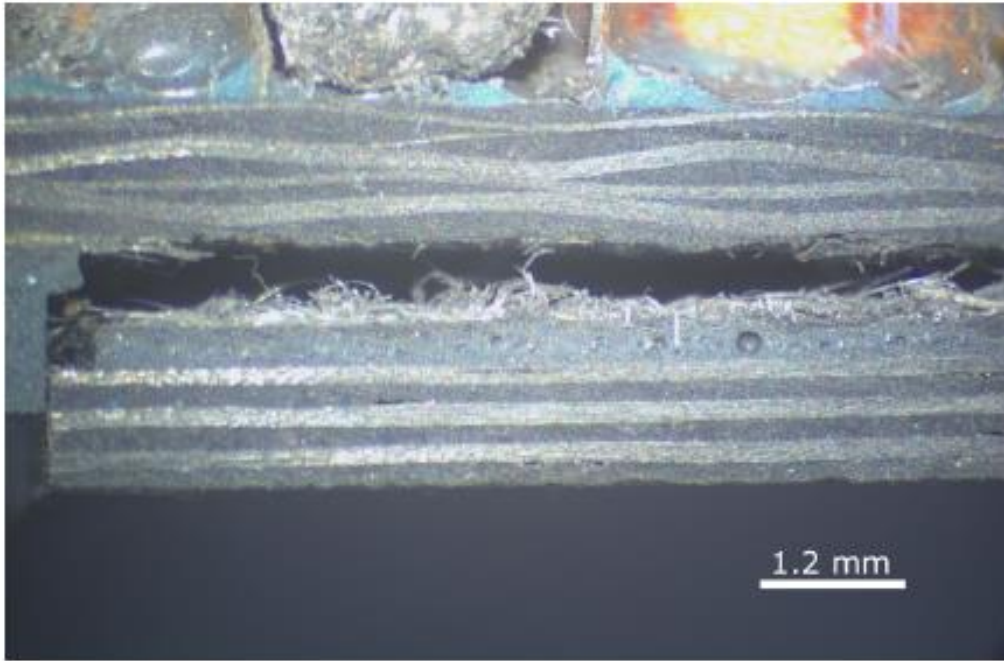


Fig. 10. Damage in a repaired sandwich specimen impacted at 30 J, a) Global view, b) Zone I: impact indentation, c) Zone II: patch debonding, d) Zone III: cracks.

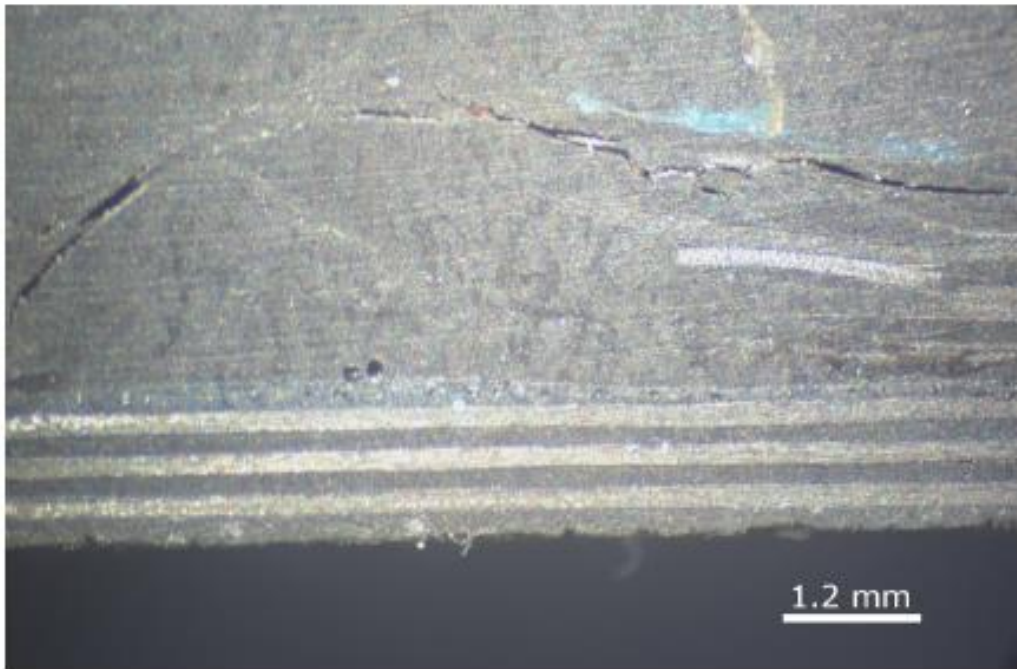


Fig. 10. Damage in a repaired sandwich specimen impacted at 30 J, a) Global view, b) Zone I: impact indentation, c) Zone II: patch debonding, d) Zone III: cracks.